Published in final edited form as:
Mol Imaging Biol. 2012 December ; 14(6): 676–687. doi:10.1007/s11307-012-0553-3.

Specific chemotaxis of magnetically labeled mesenchymal stem cells: Implications for MRI of glioma

Margaret F. Bennewitz[a], **Kevin S. Tang**[a], **Eleni A. Markakis**[b,c], and **Erik M. Shapiro**[a,b,c,*]

[a]Department of Biomedical Engineering, Yale University, 300 Cedar Street, New Haven, CT 06510, USA

[b]Molecular and Cellular MRI Laboratory, Magnetic Resonance Research Center, Department of Diagnostic Radiology, 300 Cedar Street, Yale University School of Medicine, New Haven, CT 06510, USA

[c]Yale Stem Cell Center, Yale University School of Medicine, 10 Amistad Street, New Haven, CT 06520

Abstract

Purpose—Glioblastoma multiforme (GBM) is a lethal disease, marked by infiltration of cancerous cells into the surrounding normal brain. The dire outcome of GBM patients stems in part from the limitations of current neuroimaging methods. Notably, early cancer detection methodologies are lacking, without the ability to identify aggressive, metastatic tumor cells. We propose a novel approach for tumor detection using MRI, based on imaging specific tumor tropism of mesenchymal stem cells (MSCs) labeled with micron-sized iron oxide particles (MPIOs).

Procedures—MPIO labeled and unlabeled MSCs were compared for viability, multi-lineage differentiation, and migration, where both chemotactic and chemokinetic movement were assessed in the presence of serum free medium, serum containing medium, and glioma conditioned medium. MRI was performed on agarose samples, consisting of MPIO labeled single MSCs, to confirm the capability to detect single cells.

Results—We determined that MPIO labeled MSCs exhibit specific and significant chemotactic migration towards glioma conditioned medium *in vitro.* Confocal fluorescence microscopy confirmed that MPIOs are internalized and do not impact important cell processes of MSCs. Lastly, MPIO labeled MSCs appear as *single* distinct, dark spots on T_2* weighted MRI, supporting the robustness of this contrast agent for cell tracking.

Conclusions—This is the first study to show that MPIO labeled MSCs exhibit specific tropism toward tumor-secreted factors *in vitro*. The potential for detecting single MPIO labeled MSCs provides rationale for *in vivo* extension of this methodology to visualize GBM in animal models.

Keywords

mesenchymal stem cell; glioma; iron oxide particles; chemotaxis; MRI

*Corresponding author. Magnetic Resonance Research Center, Yale School of Medicine, 300 Cedar Street, TAC N129, New Haven, CT 06519, USA; *Tel:* +1 (203)785-2899; *Fax:* +1 (203) 785-6643; erik.shapiro@yale.edu.

Conflict of Interest Authors declare that they have no conflict of interest

Introduction

Glioblastoma multiforme (GBM) is the most prevalent type of malignant glioma. Diffuse brain tumors are formed with infiltrating cells along the periphery of the tumor, which continue to invade into the surrounding normal brain. Despite the combination of surgical resection, radiation, and chemotherapy, the patient outcome for GBM remains adverse, with an average survival of only 14.6 months following diagnosis [1, 2]. The poor outcome for patients with GBM is due in part to the limitations of neuroimaging that preclude early diagnosis.

Currently, GBM is visualized using T_1 or T_2 weighted magnetic resonance imaging (MRI). T_1 methods utilize exogenous gadolinium chelates that enter the brain through highly permeable, compromised neovasculature present within the tumor [3]. Since necrosis is often a feature of GBM [4], T_1 images of these tumors typically show bright ring enhancement around the non-enhancing dead tissue [5]. T_2 methods, however, do not utilize contrast agents, but rely on intrinsic differences between edematous tumor and surrounding normal tissue; edema associated with GBM appears bright on T_2 images [6]. Both methods have several drawbacks. First, they cannot visualize nonangiogenic tumors of 1-2 mm^3, and therefore cannot provide early cancer detection. Second, they cannot visualize the infiltrating brain tumor cells characteristic of GBM that are the cause of tumor recurrence, within 2 cm of the periphery [7-9]. Third, T_1 and T_2 imaging techniques *indirectly* identify GBM through blood brain barrier (BBB) integrity and edema respectively, making interpretations about treatment effectiveness and tumor progression/recurrence challenging [10-12].

In this work, we test the validity of a new method of detecting GBM using cells as diagnostic agents. Several cell types exhibit specific tropism towards GBM, and follow metastatic outgrowths from the tumor that infiltrate the normal parenchyma, including mesenchymal stem cells (MSCs) [13, 14], neural stem cells (NSCs) [15], haematopoietic progenitor cells [16], macrophages [17, 18], lymphocytes [19], and microglia [20]. These cell types can be labeled with magnetic particles, and their migration imaged on MRI. There are several advantages in using labeled cells to migrate to GBM, including that the tumor can be imaged *directly* and *specifically*, and that eventually, anti-tumor therapeutics can be engineered into those cells. Of the cell types drawn to gliomas, MSCs are of particular interest, since they can be autologously harvested from the bone marrow or adipose tissue, expanded *in vitro*, stably labeled with magnetic particles and/or transfected with transgenes, and reintroduced back into the patient [21, 22].

MRI is ideal for tracking cell migration and homing in living organisms due to its noninvasiveness, high spatial resolution, 3D acquisition capability, and potential for serial monitoring. To enable cell tracking with MRI, cells are loaded with contrast agents. Particles of superparamagnetic iron oxide have been commonly used for this purpose, and are commercially available in different sizes. In using MRI to monitor MSC homing to brain tumors, two imaging scenarios are envisaged. In the first, large numbers of labeled cells migrate to a tumor mass, in which case, MRI detection will be straightforward. Here, MRI would detect a large area of dark contrast owing to the presence of many iron oxide labeled cells. In the second scenario, homing of low numbers of MSCs (1-5 cells) to smaller masses or even clusters of infiltrating tumor cells will require high resolution and highly sensitive MRI contrast agents for detection. In the latter case, the selection of a robust magnetic particle type for cell labeling is more important.

There are different classes of magnetic particles for MRI-based cell tracking. Ultrasmall (USPIO) and small (SPIO) superparamagnetic iron oxide particles contain <1% iron by

weight, while, micron sized particles of iron oxide, or MPIOs, contain over 34.2% iron [23]. Furthermore, the more dense packing of iron into MPIOs results in almost a 50% increase in T_2* relaxivity compared to SPIOs, when normalized for iron content [24]. Indeed, based on iron content and relaxivity, MPIOs are nearly 500-times more efficient for magnetic cell labeling than SPIOs [25]. To visualize a single cell on MRI, enough particles have to accumulate within the labeled cell to reach 1 pg of iron [26, 27]. Since one MPIO contains roughly 1.1 pg of iron, only one bead is necessary to visualize a single cell on MRI, whereas millions of (U)SPIOs are needed to reach that level of detection. Typically, (U)SPIO labeling requires the help of transfection agents [28], whereas, efficient MPIO labeling can be achieved by simple overnight incubation with a desired amount of beads/cell. Taken together, MPIOs would be the agent of choice for these endeavors.

In this work, we discovered that MPIO labeled MSCs exhibit specific and significant migration towards glioma conditioned medium *in vitro*. We also show that internalized MPIOs do not alter important cellular processes of MSCs, such as viability and multi-lineage differentiation. This is the first study to demonstrate the potential of MPIOs for tracking tumor-tropic MSCs, and that the chemoattraction between magnetically labeled MSCs and tumor conditioned medium is mediated solely by chemotactic or directional migration, and does not include any chemokinetic, or random migration interaction. These findings provide the rationale to investigate the *in vivo* use of this methodology to visualize GBM in animal models in future studies. We propose a novel, alternative method for visualizing gliomas by combining the tumor tropism of MSCs with MRI-based cell tracking. MRI of MSCs labeled with MPIOs will allow for the spatiotemporal visualization of single migrating labeled MSCs toward glioma, *in vivo*.

Materials and Methods

Cells and culture

Primary rat MSCs derived from the bone marrow of adult female Fischer 344 rats were obtained from Millipore (Cat # SCR027, Billerica, MA). The cells were maintained in low glucose DMEM without L-glutamine, supplemented with 10% fetal bovine serum (FBS), 1% L-glutamine, and 1% penicillin streptomycin (PS). Rat 9L and RG2 glioma cells (American Type Culture Collection, Manassas, VA) were cultured in high glucose DMEM, supplemented with 10% FBS and 1% PS.

Superparamagnetic iron oxide particles

Superparamagnetic MPIOs (Bangs Laboratories, IN) are comprised of an inert poly(styrene/divinylbenzene) polymer, with carboxyl functional groups on the surface. Each 1.63 m bead (Cat # ME04F) has an iron oxide core for MRI visualization, with a fluorophore incorporated into the polymeric coating for histological verification. Beads with the following fluorophores were utilized in experiments: Dragon Green (480 nm excitation, 520 nm emission) and Suncoast Yellow (540 nm excitation, 600 nm emission).

Cell labeling with MPIOs

Rat MSCs were grown until 80% confluent. To determine optimal magnetic labeling conditions, Dragon Green MPIOs, suspended in culture medium, were added to each flask at concentrations of 5, 10, 20, or 40 beads/cell. Control cells received media only. After overnight incubation with MPIOs, free beads were washed away and cells were examined on a Leica MZ16FA stereo fluorescence microscope (Leica Microsystems, Cambridge, UK). Bright field photomicrographs were acquired to visualize MPIO labeled MSCs. Inductively coupled plasma-optical emission spectrophotometry (ICP-OES) was utilized to determine the average amount of iron per MPIO labeled cell. Flow cytometry was used to determine

the percentage of labeled and viable cells (LSR II Flow Cytometer System, BD Biosciences, Bedford, MA). An additional sample was prepared with unlabeled cells, heated at 100°C for 10 minutes, to serve as the dead control. Viability was assessed using SYTOX Blue dead cell stain (Cat #S34857, Invitrogen, Carlsbad, CA) that binds to nucleic acids of cells with compromised membranes. Each sample was assayed in duplicate. Additionally, viability of unlabeled MSCs and MPIO labeled MSCs (labeled with 40 beads added/cell) was assessed using trypan blue exclusion immediately and at 1, 2, and 3 weeks following labeling to determine the impact of internalized beads over time on cell survival. Samples were assayed in triplicate.

Confocal Microscopy

MSCs were labeled overnight in T25s with Suncoast Yellow MPIOs at 40 beads added/cell. Control cells were not incubated with beads. Following trypsinization, MSCs were stained with carboxyfluorescein diacetate succinimidyl ester (CFDA-SE) (Cat # C34554, Invitrogen), which labels the cytoplasm of live cells green. The green MSCs were plated onto 2 well chamber slides and allowed to attach overnight. The next day, cells were fixed with 4% paraformaldehyde, washed with phosphate buffered saline (PBS), and mounted with ProLong Gold antifade with DAPI (Cat # P-36931, Invitrogen). Slides were imaged on a Leica TCS SP5 Spectral Confocal Microscope. Z-stacks were obtained of a confluent layer of MSCs and orthogonal cuts of the 3D stacks in two directions were used to show internalization of beads within the thickness of the cells.

MRI Single Cell Imaging with MPIOs

Unlabeled and MPIO labeled MSCs (labeled with 40 beads added/cell) were trypsinized, counted, fixed in 10% buffered formalin phosphate, and suspended in PBS. MSCs with and without beads were suspended in 1% agarose at 200,000 cells/ml; equal amounts of agarose and cell solution were added to a small glass tube, which resulted in 0.5% agarose with 100,000 cells/ml. Agarose was necessary to prevent sedimentation and promote single cell suspension. 1 mM ProHance (gadoteridol) (Bracco Diagnostics Inc, Princeton NJ) was added to the agarose solution to reduce the time for T_1 recovery, resulting in faster scan times. MRI was performed at 4.0 T on a Bruker Biospec horizontal bore spectrometer. 3D T_2* gradient echo images were acquired with the following parameters: TR = 100 msec, TE = 15 msec, FOV = 2.24 × 0.64 × 0.64 cm, matrix size = 448 × 128 × 128, Resolution = 50 μm. AMIDE (Andreas Loening, MIT) was used for processing and producing sagittal views of the samples.

Multilineage Differentiation

To assess the effect of MPIOs on the known multilineage differentiation capacity of MSCs, both unlabeled and MPIO labeled MSCs (labeled with 40 beads added/cell) were induced down adipogenic and osteogenic lineages. 50,000 rat MSCs were added to each well in 6 well plates, and grown to 80% confluency. Test wells were incubated overnight with Dragon Green MPIOs at 40 beads added/cell, while control wells received just media. The next day, all wells were washed and either adipogenic or osteogenic medium was added. Adipogenic medium was comprised of low glucose DMEM without L-glutamine, supplemented with 1 μM dexamethasone, 10 μg/ml bovine insulin, 100 μM indomethacin, 0.5 mM 3-isobutyl-1-methylxanthine, 10% FBS, 1% L-glutamine, and 1% PS, adapted from [29]. Osteogenic medium was comprised of low glucose DMEM without L-glutamine, supplemented with 50 M ascorbic acid, 10 mM β-glycerophosphate, 10 nM dexamethasone, 10% FBS, 1% L-glutamine, and 1% PS, adapted from [30]. After 3 weeks of incubation, the cells were stained with either oil red o or alizarin red, to identify adipogenic or osteogenic differentiation, respectively [29, 30]. Samples were assayed in triplicate.

The degree of adipogenic differentiation was quantified using ImageJ (NIH, Bethesda, MD). Images of oil red o stained unlabeled and MPIO labeled MSCs were thresholded to produce a binary image, with the stained regions in black. From these binary images, the % area of the black pixels was determined. The % differentiation relative to the control samples was calculated by dividing the % area for the MPIO labeled samples by the average % area for the control unlabeled samples. Eight images were assayed for both cells with and without internalized beads.

Tumor Conditioned Medium

Rat 9L and RG2 glioma cell lines were cultured to 80-90% confluency. After extensive washing in PBS to remove any traces of serum, serum free medium was added to the flasks and the cells incubated at 37°C. Twenty four or 48 hours later, the conditioned medium was collected, centrifuged at 1,000 RPM for 10 minutes to remove debris, and sterile filtered. The conditioned medium was frozen at −20°C until needed.

Chemokinesis Assay

The Radius 24-well cell migration assay (Cat # CBA-125, Cell Biolabs, San Diego, CA) was utilized to test the chemokinetic migration, or non-directional, random motion, of rat MSCs. In this assay, cells are bathed in a uniform concentration of test medium, which allows for the assessment of random motion, which is different than a chemotactic migration assay that measures specific, directional motion by providing a gradient of chemotactic factors. Each well has a gel spot of ~0.68 mm in diameter, on which cells do not attach; however, cells attach everywhere else on the bottom of the well, around the hydrogel, to form a radial gap. Once the hydrogel is dissolved, test medium is added and cells are free to migrate. Test media included serum free medium (negative control), 10% serum containing medium (positive control), and tumor conditioned media from 9L and RG2 glioma cell lines. Gap closure indicates chemokinetic migration.

The chemokinesis assay was carried out per manufacturer's instructions, with the following additional details: Passage 10 unlabeled MSCs and Suncoast Yellow MPIO labeled MSCs (labeled with 40 beads added/cell) were stained with CFDA-SE dye as in the confocal imaging section. 75,000 cells were added to each well and incubated at 37°C for 24 hours to reach desired confluence. Migration proceeded for 24 hours at 37°C, and then plates were fixed with 4% paraformaldehyde. Radial gaps were imaged immediately before migration and 24 hours after migration at 100x with an Olympus IX51 inverted fluorescence microscope (Olympus, Tokyo, Japan). The fluorescein isothiocyanate (FITC) filter was utilized to visualize the migrated green MSCs, while the red fluorescent protein (RFP) filter detected the presence of Suncoast Yellow beads inside the migrated cells. FITC and RFP images were overlayed using Adobe Photoshop CS5. The extent of gap closure was computed using ImageJ. The perimeter of the radial gap was manually traced in ImageJ, and the area of the gap for each sample was determined at 0 hours and 24 hours following migration. Percent closure was calculated for each sample by using the following equation:

$$\%\ \text{closure} = ((\text{Area}_{0\text{hrs}} - \text{Area}_{24\text{hrs}}) / \text{Area}_{0\text{hrs}}) * 100\%$$

Samples were assayed in quadruplicate.

Chemotaxis Assay

The BD Falcon HTS FluoroBlok 96 Multiwell Insert System with 8 μm pores (Cat # 351163, BD Biosciences) was used to assess the chemotactic migration of rat MSCs. In these transwell plates, a gradient forms at the membrane interface, between the cells in the

top compartment and the test mediums in the bottom compartment, to measure directional migration. The membranes in the transwell plates are coated with a dye that blocks the excitation/emission wavelengths of light between 490 nm and 700 nm. These plates allow for direct visualization of fluorescently labeled cells that have migrated to the bottom side of the membranes, without having to scrape off non-migrated cells from the top.

First, passage 9 unlabeled MSCs and Suncoast Yellow MPIO labeled MSCs (labeled with 40 beads added/cell) were stained green fluorescent with CFDA-SE dye, which has an excitation/emission spectrum of 492 nm/517 nm. Cells were resuspended in serum free medium and 50 μl (10,000 cells total) was added to each top well on the FluoroBlok plates, while 200 μl of chemoattractant solution was added to each bottom well. The same mediums used in the chemokinesis assay above were utilized in the chemotaxis assay. After a 17 hour incubation at 37°C, the FluoroBlok membranes were washed with PBS and fixed in 4% paraformaldehyde. The bottom sides of the membranes were imaged similar to the cells in the chemokinesis assay. Next, a grid was placed over each image using ImageJ and the number of cells was counted in 4 non-overlapping, adjacent fields. The average number of cells per field for each image was determined and divided by the average number of cells per field from the serum free images to calculate the chemotactic index (CI). Samples were assayed in triplicate.

Statistics

Results are shown as mean ± standard deviation. Statistical significance was determined using the unpaired two-tailed Student's t-test, where $*p < 0.05$ is significant and $**p < 0.01$ is highly significant.

Results

Cell labeling with MPIOs

Optimal magnetic labeling conditions for rat bone marrow derived MSCs were determined. The bright field photomicrographs in Figure 1a-d show successful labeling of rat MSCs with increasing amounts of added MPIOs/cell that appear as dark spots within cell boundaries. Through comparison of bright field images, it was evident that a greater number of added beads/cell resulted in enhanced labeling, or a greater amount of internalized iron/cell, as confirmed by ICP-OES (table in Figure 1). As displayed in Figure 1e-h and in the table, flow cytometry analysis showed that as the number of beads added/cell increased from 5 to 40, the percentage of cells labeled with MPIOs rose from roughly 40% to 76%, while viability remained consistently high (between 96%-98%). Unlabeled cells and heat-killed cells were used as controls, and exhibited high (98.7%) and low viability (<1%), respectively (data not shown). Over the course of 3 weeks in culture, viability was found to be ≥ 96% for cells with and without endocytosed beads, with the difference in viability between control unlabeled and MPIO labeled MSCs not being statistically significant (data not shown). Since 40 beads added/cell resulted in the greatest percentage of labeled MSCs, the maximum average number of endocytosed beads per labeled cell, and a high percentage of viability, this labeling paradigm was utilized in all subsequent experiments.

Confocal Microscopy

Confocal microscopy was utilized to evaluate whether MPIOs were endocytosed within cells or associated with the cell surface. Figure 2 shows that the morphology of control unlabeled MSCs (2a) and MPIO labeled MSCs (2b) appears similar. More importantly, Figure 2b also displays two orthogonal cuts through an acquired z-stack, highlighting a fully internalized bead present throughout the thickness of the cell (as shown by the white arrows). Surface associated beads, in contrast, would appear on top of the cell in these profile cuts and do not

overlap with the cell thickness. Multiple particles were analyzed and confocal imaging confirmed that most MPIOs were endocytosed within MSCs, with only a small fraction being surface associated beads.

MRI Single Cell Imaging with MPIOs

T_2* weighted MRI was utilized to demonstrate the robustness of MPIOs to delineate single labeled MSCs in an agarose suspension. Figure 3 shows that control unlabeled cells, without any internalized iron, did not significantly impact the signal intensity of the sample (3a), whereas the same number of MSCs labeled with MPIOs induced distinctive, single dark spots throughout the sample (3b); each hypointense spot represents a single MSC labeled with multiple MPIOs. MRI confirmed that it is possible to distinguish MPIO labeled MSCs from unlabeled cells using T_2* weighted gradient echo imaging.

MSC Multilineage Differentiation

While in this study, we are not intending or expecting MSCs to differentiate into tissue specific cells, it is important to determine the impact of MPIOs on cellular processes. Figure 4 shows robust adipogenesis and osteogenesis for both unlabeled MSCs (a,d) and MPIO labeled MSCs (b,e), indicating that internalized MPIOs (shown in green) do not affect the ability of MSCs to differentiate into fat and bone cells. It may appear in Figure 4b that many extracellular beads are present, however, these beads are internalized within undifferentiated MSCs that do not possess any oil red o staining. In addition, the degree of adipogenic staining for MSCs with and without internalized beads was quantified using ImageJ. Figure 4c illustrates that there was no significant difference between the amount of adipogenic differentiation of unlabeled and MPIO labeled MSCs, which further supports the negligible impact of MPIOs on multilineage differentiation.

Chemokinesis Assay

The Radius 24-well cell migration assay was utilized to evaluate chemokinetic migration, or non-directional, random motion of unlabeled and MPIO labeled MSCs. As shown in Figure 5a, the only condition that produced a chemokinetic response was the positive control (10% serum containing medium), as evidenced by the disorganized encroachment of cells into the interior portion of the radial gap after 24 hours. The % closure for MPIO labeled MSCs in serum positive medium was similar to unlabeled MSCs: 55 ± 7% compared to 51 ± 5%, respectively. The radial gaps in the negative control (serum free medium) and tumor conditioned mediums remained perfectly intact after 24 hours (5b), and therefore did not indicate any chemokinetic migration. A lack of random migration of MSCs in tumor conditioned mediums confirmed that any migration towards these solutions in the chemotactic assay would indeed be directional and specific; the desired interaction between MSCs and tumor cells should be as specific as possible, since we aim to use MSCs as a diagnostic tool for accurately delineating GBM.

Chemotaxis Assay

The chemotactic, or directional, migration of unlabeled and MPIO labeled MSCs was evaluated using the FluoroBlok 96 Multiwell Insert System. Representative subsections of the total area of migrated cells are shown in Figure 6 for each medium type tested. The serum free medium had very few migrated cells (6a,b) in contrast to 10% serum containing medium, which exhibited a robust migration response (6c,d). Conditioned medium from the 9L and RG2 glioma cell lines also produced chemotactic migration (6e-j), with the exception of the RG2 48 hour samples (6k,l). In addition, chemotactic migration between cells ± MPIO (MPIOs shown in red) for each condition appeared similar. Insets in d, f, h, and j highlight migrated cells containing MPIOs. Confirming the presence of MPIOs within

migrated cells was crucial to assessing magnetically labeled MSC functionality, since 24% of MSCs still remained unlabeled after incubation with MPIOs.

Chemotactic migration towards 10% serum containing medium, 9L 24 hour, 9L 48 hour, and RG2 24 hour glioma conditioned medium was highly significant (**$p < 0.01$) compared to serum free medium, as graphically summarized in Figure 6. The highest chemotactic index (CI) was exhibited by 10% serum containing medium, followed by RG2 24 hour and 9L 24/48 hour conditioned medium, which produced a response between 30%-45% of the positive control. It is important to note that the migration towards the positive control was so high because it contained a combination of chemotactic as well as chemokinetic migration, whereas the migration towards glioma conditioned medium was purely chemotactic. Furthermore, the CI for unlabeled and MPIO labeled MSCs was not significantly different for any medium type tested, indicating that internalized MPIOs did not affect MSC chemotactic migration. Most importantly, we have shown that magnetically labeled MSCs are attracted to glioma conditioned medium *in vitro*, and that this migration is robust, specific, and directional.

Discussion

Recently, MPIOs have been utilized for tracking transplanted MSCs with MRI for a number of applications with promising results, including periventricular white matter injury [31], myocardial infarction [32], cartilage regeneration [33], and spinal cord injury [34]. However, there have been no studies using MPIO labeled MSCs to delineate and monitor GBM. In this work, we demonstrate for the first time that MPIO labeled MSCs exhibit specific migration towards tumor conditioned medium, and further show that the response is chemotactic, not chemokinetic. The goal of our study was to provide the rationale of using the larger, micron-sized iron oxide particles to track MSC tropism to glioma *in vitro,* before moving into animals in future experiments.

We assessed two different migration phenomena of magnetically labeled MSCs: chemotaxis, or directional and specific movement, and also chemokinesis, or non-directional and random movement. We show that MPIO labeled MSCs migrate specifically and directionally (via chemotaxis not chemokinesis) toward glioma conditioned medium from 9L and RG2 cell lines *in vitro*. The finding that MSCs are specifically attracted to gliomas was important because we aim to use MSCs as a diagnostic tool for delineating GBM, and thus need the MSCs to directly target the tumor cells without any random deviation away into the normal brain.

In the transwell assay, we found that MPIO labeled MSC migration was significant towards 9L 24 hour, 9L 48 hour, and RG2 24 hour tumor conditioned medium. Since the conditioned medium did not contain any serum, the MSC chemotaxis towards those solutions was due to the chemoattractants present within the medium that had been produced by the glioma cell lines. Several studies propose that MSC tumor tropism may be mediated by the following factors: platelet-derived growth factor BB (PDGF-BB), epidermal growth factor (EGF), hepatocyte growth factor (HGF), insulin-like growth factor (IGF), stromal cell-derived factor 1 alpha (SDF-1), and monocyte chemotactic protein-1 (MCP-1), among others [35-38]. Increasing the expression of chemoattractant receptors of interest, which are present on the surface of MSCs, could serve to intensify *in vivo* MSC migration to gliomas. Studies have found that enhancement of CXCR4 (the receptor for SDF-1) on MSCs has improved migration to the heart following myocardial infarction and also to the bone marrow following irradiation.[39] Overexpression has been achieved through incubation of MSCs with various cytokines [40] or through retroviral transduction [41].

The only tumor conditioned medium that did not induce significant MPIO labeled MSC chemotaxis was RG2 tumor medium collected after 48 hours. It is likely that this conditioned medium was nutrient depleted due to the rapid expansion of RG2 cells in culture (RG2 cells grew faster than 9L), as supported by our observation of a change in color (and thus pH) of the medium from pink to orange. It is also possible that the concentrations of chemoattractants secreted by the RG2 cells after 48 hours may not be optimal for MSC chemotaxis; specifically, the concentrations of the factors secreted may be too high. Xu et al. [36] and Ozaki et al. [37] have shown that for chemotaxis of MSCs towards single factors *in vitro*, there exists a bell shaped curve, with an optimal concentration causing maximum migration, and a steady decline in chemoattraction for any concentrations above the optimum.

We acknowledge that the chemotactic assay was an *in vitro* experiment, using conditioned medium from rat glioma cell lines, and has some inherent limitations. First, the tumor conditioned medium was collected under static conditions, with the concentration of chemoattractants most likely dependent on the volume of collection media and the number of plated cells secreting them. While this does not represent the dynamic *in vivo* environment, it provides rationale to pursue the *in vivo* extension of this methodology. Second, we have only tested the chemoattraction of MSCs to medium conditioned only by tumor cells. The *in vivo* tumor environment is more complex than this, with other cell types making up the glioma (and secreting their own chemoattractants) including astrocytes, microglia, endothelial cells, and stromal cells. However, for small clusters of infiltrating tumor cells, this may represent a reasonable cellular makeup.

Other studies have investigated the specificity of MSC migration towards tumors both *in vitro* and *in vivo*. In standard chemotaxis transwell assays, MSCs were observed to migrate significantly towards various glioma cell lines grown in the bottom of the transwells including F98, U87MG, LN18, U138, and U251 [42-44]. In contrast, MSC migration was found to be negligible towards lysis of normal brain tissue and towards conditioned medium from noncancerous cells, such as astrocytes and fibroblasts [35, 44, 45]. In addition, *in vivo* studies found that intracranially or intra-arterially injected MSCs will home specifically to the main tumor mass and infiltrating glioma cells, but largely avoid normal tissue adjacent to tumors and the contralateral brain [35, 46]. These results complement our study to further establish that MSCs have the capability to specifically home and migrate to glioma versus other cells.

Critical to the use of magnetically labeled MSCs as a diagnostic tool is the assurance that the magnetic label is fully internalized within the cell, and is non-interfering in important cellular processes. MPIOs are heavy and will sink to the bottom of the cell culture flask during overnight labeling; cells will fully internalize some of these beads by endocytosis, while other beads remain on the cell surface, and must be washed away extensively with PBS. Any beads left that are weakly associated to the cell surface could either fall off through trypsinization or detach *in vivo* and be picked up by other cells within the body, most likely immune cells. The dark spots on T_2* weighted MRI from the magnetically labeled immune cells would appear similar to the MPIO labeled MSCs, confounding diagnostic imaging results. Consequently, we confirmed with confocal imaging that most MPIOs were completely endocytosed within the MSCs, and that the presence of surface associated beads was minimal. Although most beads were endocytosed within cells, MSCs were observed to label non-uniformly, where the maximum percentage of labeled cells reached 76% in the highest labeling condition. This points to the heterogeneous nature of MSCs as a whole, and indicates that magnetic cell sorting may be worth pursuing to enrich the fraction of labeled cells even further in future experiments. In addition, we have shown that internalized MPIOs did not affect MSC functionality. Specifically, unlabeled and

magnetically labeled MSCs had similar viability, differentiation capacity, and migration response. Furthermore, we showed the robustness of this contrast agent for cell tracking by demonstrating the ability to view MPIO labeled single cells in agarose phantoms on T_2* weighted MRI, similar to Shapiro et al. [26].

Two previous studies, by Chien et al. [42] and Wu et al. [44], have investigated migration of nanometer sized SPIO labeled MSCs towards glioma. Chien et al. [42] found that human MSCs, labeled with SPIOs, migrated towards glioma (U87MG cells) *in vitro* and that SPIO labeling did not negatively affect the extent of cell movement compared to the unlabeled control; however, the presence of SPIOs within migrated cells was not confirmed, and the mechanism of MSC migration (chemotactic vs. chemokinetic) was not determined. Still, the *in vivo* work from these two studies does show some promising preliminary results: Iron labeled MSCs were visible on MRI as dark contrast regions near/within the glioma, providing evidence that SPIO labeled MSCs are attracted to gliomas *in vivo.* Yet, this tropism was most convincingly shown through histology in both studies. Even so, both experiments utilized 1.5 T imaging, resulting in poor quality images with low resolution. In addition, the use of SPIOs requires the presence of tens to hundreds of thousands of cells for robust visualization. This problem does not occur with MPIOs, which have enough iron in one bead to be visualized on T_2* weighted MRI [26, 27] and allow for robust single cell detection and tracking *in vivo* [47]. While both papers are important proofs of principle, the use of low field MRI and SPIO does not allow delineation of the whole tumor with MSCs, nor are the images clear enough to distinguish or quantify single labeled MSCs. Consequently, there is room for improvement in this field of research.

Our strategy can be manipulated to form a cellular “theragnostic” approach to treating and diagnosing GBM, whereby MSCs would be used as agents to provide treatment through genetic engineering, and at the same time, enable visualization of the target via MRI-based cell tracking. Various studies have begun to investigate a therapeutic approach using genetically engineered MSCs as vehicles to specifically target and deliver antitumor factors to gliomas. In particular, these MSCs have been utilized to deliver interferon-β [35, 48], interleukin-2 (IL-2) [13], IL-7 [49], IL-18 [50], Δ24-RGD [51], and secretable tumor necrosis factor-related apoptosis-inducing ligand (S-TRAIL) [52, 53] to gliomas, which have resulted in a decrease in tumor size and an increase in survival for treated animals over controls. Still missing in these treatment modalities is a method for monitoring transplanted cells *in vivo*. Therefore, the combination of the diagnostic capability of MRI cell tracking with genetic engineering of antitumor factors would provide a valuable tool to combat GBM.

The ultimate utility of MSCs in glioma diagnosis and/or treatment remains to be determined, however, we envision the use of theragnostic MSCs in patients who are already diagnosed with GBM or who may be predisposed to acquiring the disease. Since it is known that MSCs are also attracted to tissue damage and inflammation, such as stroke [54], periventricular white matter injury [31], myocardial infarction [32], and wounded skin [55], it would be challenging to use labeled MSCs to perform differential diagnosis between these conditions, which most likely share similar chemoattractants. After GBM diagnosis, theragnostic MSCs would be utilized to track and target the main tumor mass and invasive tumor cells that have infiltrated the normal brain. There is even evidence of enhanced MSC migration to irradiated tumors [56] and tissues [57], due to increased cytokine expression, which can be exploited to create a more efficient treatment paradigm for GBM patients.

MSCs are proposed to home and transmigrate across endothelial cells in a similar fashion to leukocytes, due to shared chemokine and adhesion receptors [58]. Therefore, we envision systemic injection of MSCs, particularly intra-arterial delivery, to GBM patients. Studies

have shown that intravenous injection of MSCs results in substantial trapping of cells within the lungs, liver, and spleen [59-61]. Alternatively, intra-arterial injection allows more direct access of MSCs to the brain through bypassing systemic organs, thus causing greater MSC cerebral engraftment, as confirmed by Walczak et al. [54] in a stroke model. Once in the brain, Walczak et al. [54] have shown that MSCs will localize to the cerebral capillaries within ischemic regions one day after injection, but extravasate to enter the brain parenchyma within ten days following injection. A similar paradigm seems reasonable for MSC homing within the tumor environment. MSCs are proposed to be neoangiotropic [62] because they can associate along newly formed vasculature within the tumor bed [44]. As a result, MSCs are thought to share characteristics with pericytes [46]. In addition to distributing throughout the tumor, MSCs have been observed to migrate towards single and small groups of infiltrative glioma cells [44, 46], which have no developed vasculature, indicating that MSCs do transmigrate across endothelial cells into the brain parenchyma.

As a combination approach, theragnostic cells can provide several advantages over current methods in our proposed paradigm. Specific tumor tropism of genetically engineered MSCs will provide more localized treatment, resulting in less damage to normal tissue and thus reduced side effects. Internalized magnetic particles will allow for tracking of therapeutic cells and hence detection of cancerous and metastatic cells, providing the possibility of targeting infiltrative cells prior to recurrence.

Conclusions

In summary, we have shown the promise of utilizing MPIOs to label and track the migration of MSCs towards glioma. MPIOs achieved efficient labeling of MSCs without the need for transfection agents, and did not affect important cell processes of viability, differentiation, and migration *in vitro*. In addition, glioma conditioned medium caused directional and specific chemotaxis of MPIO labeled MSCs in the transwell assay. Our study provides the feasibility of combining MRI-based cell tracking with the specific tumor tropism of MSCs to delineate GBM *in vivo.* A theragnostic approach can also be created by genetically engineering magnetically labeled MSCs to produce antitumor factors to provide treatment as well as visualization of the target.

Acknowledgments

This research was supported by NIH grant DP2 OD004362. We thank Dr. Diane Krause, Yale University School of Medicine, for helpful discussions and Mr. Thomas Ardito, Yale Stem Cell Center, for confocal expertise.

References

[1]. Stupp R, Mason W, van der Bent M, Weller M, Fisher B, Taphoorn M. Radiotherapy plus concomitant and adjuvant temozolamide for glioblastoma. N Engl J Med. 2005; 352:987–996. [PubMed: 15758009]

[2]. Jansen E, Dewit L, van Herk M, Bartelink H. Target volumes in radiotherapy for high-grade malignant glioma of the brain. Radiother Oncol. 2000; 56:151–156. [PubMed: 10927133]

[3]. Sage M. Blood-brain barrier: phenomenon of increasing importantce to the imaging clinician. AJF AM J Roentgenol. 1982; 138:887–898.

[4]. Pierallini A, Bonamini M, Pantano P. Radiological assessment of necrosis in glioblastoma: variability and prognostic value. neuroradiology. 1998; 40:150–153. [PubMed: 9561517]

[5]. Carter R, Pretorius P. The use of CT and MRI in the characterization of intracranial mass lesions. Imaging. 2007; 19:173–184.

[6]. Mechtler L. Neuroimaging in Neuro-Oncology. Neurol Clin. 2008; 27:171–201. [PubMed: 19055979]

[7]. Strupp R, Hegi M, Glibert M, Chakravarti A. Chemoradiotherapy in malignant glioma: standard of care and future directions. J Clin Oncol. 2007; 16:1405–1409.

[8]. Liang B, Thornton A, Sandler H, Greenberg H. Malignant astrocytomas: focal tumor recurrence after focal external beam radiation therapy. J Neurosurg. 1991; 75:559–563. [PubMed: 1653309]

[9]. Allard E, Passirani C, Benoit J. Convection-enhanced delivery of nanocarriers for the treatment of brain tumors. Biomaterials. 2009; 30:2303–2318.

[10]. Clarke J, Chang S. Pseudoprogression and pseudoresponse: challenges in brain tumor imaging. Curr Neurol Neurosci. 2009; 9:241–246.

[11]. Jacobs A, Kracht L, Gossmann A, et al. Imaging in neurooncology. NeuroRx. 2005; 2:333–347. [PubMed: 15897954]

[12]. Yang I, Aghi M. New advances that enable identification of glioblastoma recurrence. Nat Rev Clin Oncol. 2009; 6:648–657. [PubMed: 19806145]

[13]. Nakamura K, Ito Y, Kawano Y, et al. Antitumor effect of genetically engineered mesenchymal stem cells in a rat glioma model. Gene Ther. 2004; 11:1155–1164. [PubMed: 15141157]

[14]. Zhang Z, Jiang Z, Jiang F, et al. In vivo magnetic resonance imaging tracks adult neural progenitor cell targeting of brain tumor. Neuroimage. 2004; 23:281–287. [PubMed: 15325375]

[15]. Aboody K. Neural stem cells display extensive tropism for pathology in adult brain: evidence from intracranial gliomas. Proc Natl Acad Sci USA. 2000; 97:12846–12851. [PubMed: 11070094]

[16]. Tabatabai G, Bahr O, Mohle R, Eyupoglu I, Boehmler A, Wischhusen J. Lessons from the bone marrow: how malignant gliomas attract adult haematopoietic progenitor cells. Brain. 2005; 128:2200–2211. [PubMed: 15947066]

[17]. Badie B, Schartner J. Flow cytometric characterization of tumor-associated macrophages in experimental gliomas. Neurosurgery. 2000; 46:957–961. [PubMed: 10764271]

[18]. Strik H, Stoll M, Meyermann R. Immune cell infiltration of intrinsic and metastatic intracranial tumors. Anticancer Res. 2004; 24:37–42. [PubMed: 15015573]

[19]. Watanabe T, Tanaka R, Taniguchi Y, Yamamoto K, Ono K, Yoshida S. The role of microglia and tumor-primed lymphocytes in the interaction between T lymphocytes and brain endothelial cells. J Neuroimmunol. 1998; 81:90–97. [PubMed: 9521610]

[20]. Badie B, Schartner J. Role of microglia in glioma biology. Microsc Res Tech. 2001; 54:106–113. [PubMed: 11455617]

[21]. Birnbaum T, Roider J, Schankin C, et al. Malignant gliomas actively recruit bone marrow stromal cells by secreting angiogenic cytokines. J Neurooncol. 2007; 83:241–247. [PubMed: 17570034]

[22]. Corsten M, Shah K. Therapeutic stem-cells for cancer treatment: hopes and hurdles in tactical warfare. Lancet Oncol. 2008; 9:376–384. [PubMed: 18374291]

[23]. Shapiro, E.; Koretsky, A. Micron-Sized Iron Oxide Particles (MPIOs) for Cellular Imaging: More Bang for the Buck Springer Science+Business Media. LLC; New York: 2008.

[24]. Hinds K, Hill J, Shapiro E, et al. Highly efficient endosomal labeling of progenitor and stem cells with large magnetic particles allows magnetic resonance imaging of single cells. Blood. 2003; 102:867–872. [PubMed: 12676779]

[25]. Nkansah M, Thakral D, Shapiro E. Magnetic poly(lactide-co-glycolide) and cellulose particles for MRI-based cell tracking. Magn Reson Med. 2011; 65:1776–1785. [PubMed: 21404328]

[26]. Shapiro E, Skrtic S, Sharer K, Hill J, Dunbar C, Koretsky A. MRI detection of single particles for cellular imaging. Proc Natl Acad Sci USA. 2004; 101:10901–10906. [PubMed: 15256592]

[27]. Shapiro E, Skrtic S, Koretsky A. Sizing it up: cellular MRI using micron-sized iron oxide particles. Magn Reson Med. 2005; 53:329–338. [PubMed: 15678543]

[28]. Kalish H, Arbab A, Miller B, et al. Combination of transfection agents and magnetic resonance contrast agents for cellular imaging: relationship between relaxivities, electrostatic forces, and chemical composition. Magn Reson Med. 2003; 50:275–282. [PubMed: 12876703]

[29]. Xin-Qin Kang W-JZ, Tu-Sheng Song, Xiao-Li Xu, Xiao-Jiang Yu, Dong-Ling Li, Ke-Wei Meng, Sheng-Li Wu, Zhi-Ying Zhao. Rat bone marrow mesenchymal stem cells differentiate into hepatocytes in vitro. World Journal of Gastroenterology. 2005; 11:3479–3484. [PubMed: 15948259]

[30]. Naresh, Polisetti CVG.; Babu, Phanithi Prakash; Vemuganti, Geeta K. Isolation, characterization and differentiation potential of rat bone marrow stromal cells. Neurology India. 2010; 58:201–208. [PubMed: 20508336]

[31]. Chen A, Siow B, Blamire A, Lako M, Clowry G. Transplantation of magnetically labeled mesenchymal stem cells in a model of perinatal brain injury. Stem Cell Res. 2010; 5:255–266. [PubMed: 20875955]

[32]. Ma G, QI C, Liu N, et al. Efficiently tracking of stem cells *in vivo* using different kinds of superparamagnetic iron oxide in swine with myocardial infarction. Chin Med J. 2011; 124:1199–1204. [PubMed: 21542996]

[33]. Saldanha K, Doan R, Ainslie K, Desai T, Majumdar S. Micrometer-sized iron oxide particle labeling of mesenchymal stem cells for magnetic resonance imaging-based monitoring of cartilage tissue engineering. Magn Reson Imaging. 2011; 29:40–49. [PubMed: 20863643]

[34]. Gonzalez-Lara L, Xu X, Hofstetrova K, et al. The use of cellular magnetic resonance imaging to track the fate of iron-labeled multipotent stromal cells after direct transplantation in a mouse model of spinal cord injury. Mol Imaging Biol. 2010 Online, ahead of print.

[35]. Nakamizo A, Marini F, Amano T, et al. Human bone marrow-derived mesenchymal stem cells in the treatment of gliomas. Cancer Res. 2005; 65:3307–3318. [PubMed: 15833864]

[36]. Xu F, Shi J, Yu B, Ni W, Wu X, Gu Z. Chemokines mediate mesenchymal stem cell migration toward gliomas in vitro. Oncology reports. 2010; 23:1561–1567. [PubMed: 20428810]

[37]. Ozaki Y, Nishimura M, Sekiya K, et al. Comprehensive analysis of chemotactic factors for bone marrow mesenchymal stem cells. Stem Cells and Development. 2007; 16:119–129. [PubMed: 17348810]

[38]. Ponte A, Marais E, Gallay N, et al. The in vitro migration capacity of human bone marrow mesenchymal stem cells: comparison of chemokine and growth factor chemotactic activities. Stem Cells. 2007; 25:1737–1745. [PubMed: 17395768]

[39]. Kollar K, Cook M, Atkinson K, Brooke G. Molecular mechanisms involved in mesenchymal stem cell migration to the site of myocardial infarction. Int J Cell Bio. 2009; 2009:904682. [PubMed: 20130773]

[40]. Shi M, Li J, Liao L, et al. Regulation of CXCR4 expression in human mesenchymal stem cells by cytokine treatment: role in homing efficiency in NOD/SCID mice. Haematologica. 2007; 92:897–904. [PubMed: 17606439]

[41]. Cheng Z, Ou L, Zhou X, et al. Targeted migration of mesenchymal stem cells modified with CXCR4 gene to infarcted myocardium improves cardiac performance. Mol Ther. 2008; 16:571–579. [PubMed: 18253156]

[42]. Chien L, Hsiao J, Hsu S, et al. In vivo magnetic resonance imaging of cell tropism, trafficking mechanism, and therapeutic impact of human mesenchymal stem cells in a murine glioma model. Biomaterials. 2011; 32:3275–3284. [PubMed: 21295344]

[43]. Kim D, Kim J, Lee J, et al. Overexpression of CXC chemokine receptors is required for the superior glioma-tracking property of umbilical cord blood-derived mesenchymal stem cells. Stem Cells and Development. 2009; 18:511–519. [PubMed: 18624673]

[44]. Wu X, Hu J, Zhou L, et al. In vivo tracking of superparamagnetic iron oxide nanoparticle-labeled mesenchymal stem cell tropism to malignant gliomas using magnetic resonance imaging. J Neurosurg. 2008; 108:320–329. [PubMed: 18240929]

[45]. Park S, Ryu C, Kim S, et al. CXCR4-transfected human umbilical cord blood-derived mesenchymal stem cells exhibit enhanced migratory capacity toward gliomas. International Journal of Oncology. 2011; 38:97–103. [PubMed: 21109930]

[46]. Bexell D, Gunnarsson S, Tormin A, et al. Bone marrow multipotent mesenchymal stroma cells act as pericyte-like migratory vehicles in experimental gliomas. Cell Therapy. 2008; 17:183–190.

[47]. Shapiro E, Sharer K, Skrtic S, Koretsky A. In vivo detection of single cells by MRI. Magn Reson Med. 2006; 55:242–249. [PubMed: 16416426]

[48]. Studeny M, Marini F, Champlin R, Zompetta C, Fidler I, Andreeff M. Bone marrow-derived mesenchymal stem cells as vehicles for interferon-β delivery into tumors. Cancer Res. 2002; 62:3603–3608. [PubMed: 12097260]

[49]. Gunnarsson S, Bexel D, Svensson A, Siesjo P, Darabi A, Bengzon J. Intratumoral IL-7 delivery by mesenchymal stromal cells potentiates IFNγ-transduced tumor cell immunotherapy of experimental glioma. J Neuroimmunol. 2010; 218:140–144. [PubMed: 19914721]

[50]. Xu G, Jiang X, Xu Y, et al. Adenoviral-mediated interleukin-18 expression in mesenchymal stem cells effectively suppresses the growth of gliomas in rats. Cell Bio Int. 2009; 33:466–474. [PubMed: 18725309]

[51]. Yong R, Shinojima N, Fueyo J, et al. Human bone marrow–derived mesenchymal stem cells for intravascular delivery of oncolytic adenovirus Δ24-RGD to human gliomas. Cancer Res. 2009; 69:8932–8940. [PubMed: 19920199]

[52]. Menon L, Kelly K, Yang H, Kim S, Black P, Carroll R. Human bone marrow-derived mesenchymal stromal cells expressing S-TRAIL as a cellular delivery vehicle for human glioma therapy. Stem Cells. 2009; 27:2320–2330. [PubMed: 19544410]

[53]. Sasportas L, Kasmieh R, Wakimoto H, et al. Assessment of therapeutic efficacy and fate of engineered human mesenchymal stem cells for cancer therapy. PNAS. 2009; 106:4822–4827. [PubMed: 19264968]

[54]. Walczak P, Zhang J, Gilad A, et al. Dual-modality monitoring of targeted intraarterial dlivery of mesenchymal stem cells after transient ischemia. Stroke. 2008; 39:1569–1574. [PubMed: 18323495]

[55]. Sasaki M, Abe R, Fujita Y, Ando S, Inokuma D, Shimizu H. Mesenchymal Stem Cells Are Recruited into Wounded Skin and Contribute to Wound Repair by Transdifferentiation into Multiple Skin Cell Type. The Journal of Immunology. 2008; 180:2581–2587. [PubMed: 18250469]

[56]. Klopp A, Spaeth E, Dembinski J, et al. Tumor irradiation increases the recruitment of circulating mesenchymal stem cells into the tumor microenvironment. Cancer Res. 2007; 67:11687–11695. [PubMed: 18089798]

[57]. Francois S, Bensidhoum M, Mouiseddine M, et al. Local irradiation not only induces homing of human mesenchymal stem cells at exposed sites but promotes their widespread engraftment to multiple organs: a study of their quantitative distribution after irradiation damage. Stem Cells. 2006; 24:1020–1029. [PubMed: 16339642]

[58]. Henschler R, Deak E, Seifried E. Homing of Mesenchymal Stem Cells. Transfusion Medicine and Hemotherapy. 2008; 35:306–312. [PubMed: 21512647]

[59]. Kraitchman D, Tatsumi M, Glison W, et al. Dynamic imaging of allogeneic mesenchymal stem cells trafficking to myocardial infarction. Circulation. 2005; 112:1451–1461. [PubMed: 16129797]

[60]. Hauger O, Frost E, van Heeswijk R, et al. MR evaluation of the glomerular homing of magnetically labeled mesenchymal stem cells in a rat model of nephropathy. Radiology. 2006; 238:200–210. [PubMed: 16373768]

[61]. Gao J, Dennis J, Muzic R, Lundberg M, Caplan A. The dynamic in vivo distribution of bone marrow-derived mesenchymal stem cells after infusion. Cells Tissues Organs. 2001; 169:12–20. [PubMed: 11340257]

[62]. Bexell D, Scheding S, Bengzon J. Toward Brain Tumor Gene Therapy Using Multipotent Mesenchymal Stromal Cell Vectors. Molecular Therapy. 2010; 18:1067–1075. [PubMed: 20407426]

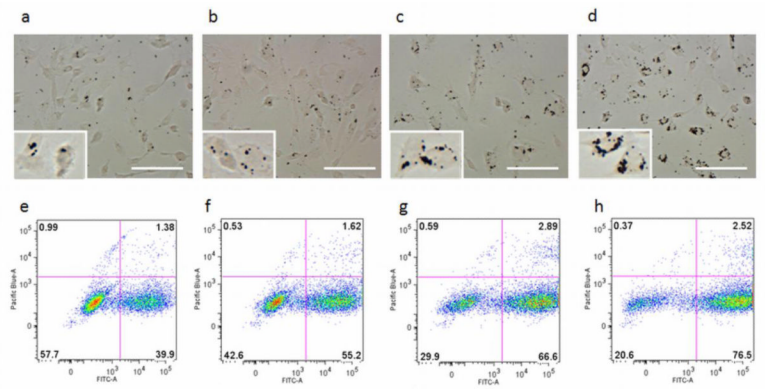

MSC labeling and viability for increasing amounts of added MPIOs

Beads added/cell	% Labeled cells	Ave iron (pg)/labeled cell	Ave # beads/labeled cell	% Viability
5	40 ± 0.4	5 ± 0.8	5	98 ± 0.4
10	56 ± 0.1	6 ± 1.4	6	98 ± 0.03
20	67 ± 0.8	9 ± 0.4	8	97 ± 0.5
40	76 ± 0.5	14 ± 0.4	13	96 ± 0.9

Figure 1.

Bright field photomicrograph and corresponding flow cytometry plot for rat MSCs labeled with a,e) 5 beads/cell b,f) 10 beads/cell c,g) 20 beads/cell and d,h) 40 beads/cell. Insets are magnified images of a small number of cells containing internalized beads for each labeling condition, with MPIOs shown in black in a-d). The FITC-A channel displays MPIO cell labeling and the Pacific Blue-A channel displays viability. The table shows MSC labeling and viability for increasing amounts of added MPIOs/cell; the values presented are mean ± standard deviation. Scale bars shown are 100 μm.

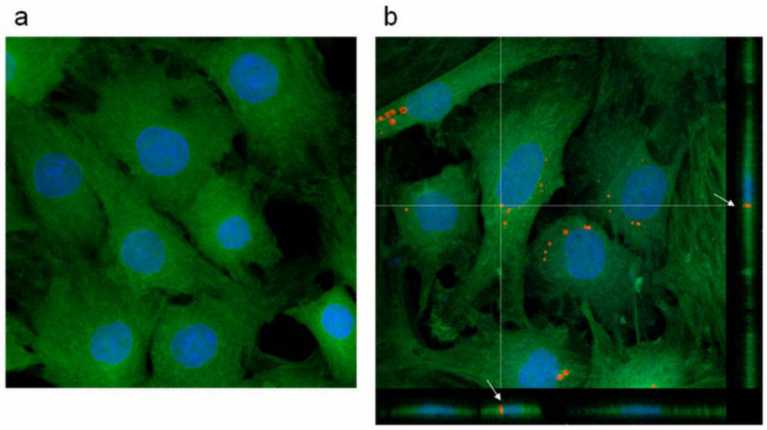

Figure 2.
Confocal images of a) unlabeled and b) MPIO labeled MSCs. The cytoplasm of MSCs is shown in green, nuclei in blue, and MPIOs in red. Note how the orthogonal projections through the z-stack show a representative fully internalized particle, as marked by the white arrows in b).

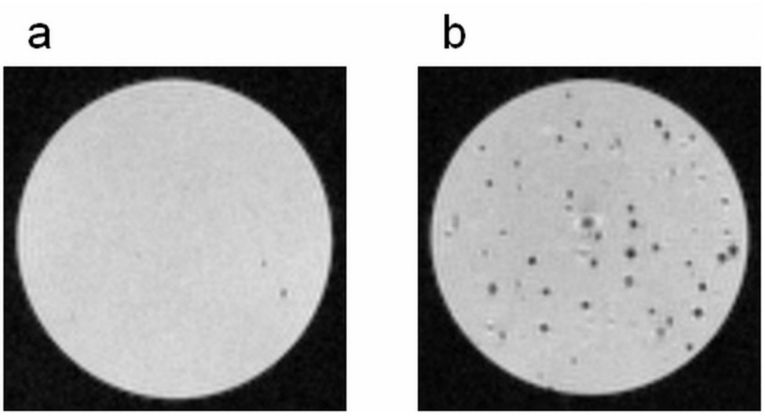

Figure 3.
T_2* weighted MRI of single cell suspensions of a) unlabeled MSCs and b) MPIO labeled MSCs in agarose. Cells without internalized iron created minimal signal loss (a), whereas the MSCs labeled with MPIOs induced single, distinctive dark spots throughout the sample (b). Each dark spot corresponds to an MSC with several internalized MPIOs. The MRI images were acquired at a resolution of 50 m.

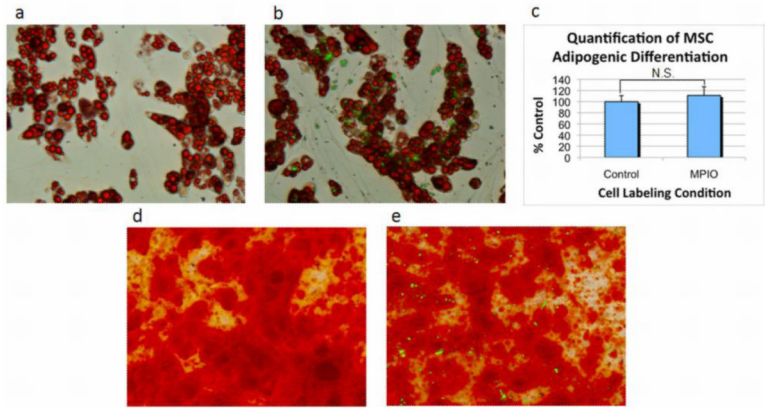

Figure 4.

Bright field photomicrograph with fluorescence overlay of adipogenic and osteogenic differentiation of unlabeled and MPIO labeled MSCs. Oil red o staining confirmed adipogenic differentiation of a) unlabeled and b) MPIO labeled MSCs. The degree of adipogenic differentiation for cells with and without endocytosed particles was quantified using ImageJ and is shown in c). N.S. indicates not significantly different. Alizarin red staining confirmed osteogenic differentiation of d) unlabeled and e) MPIO labeled MSCs. MPIOs are shown in green.

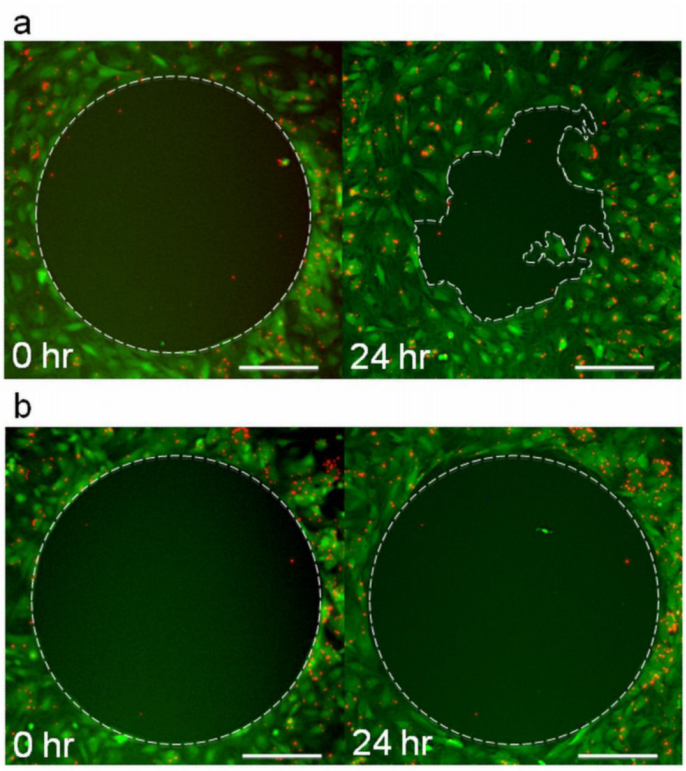

Figure 5.
Fluorescence photomicrographs of chemokinetic migration of MPIO labeled MSCs after 0 and 24 hours of incubation in a) 10% serum containing medium and b) 9L 48 hour tumor conditioned medium. Cells are shown in green and MPIOs in red. Only MSCs in serum containing medium a) showed a chemokinetic response, which resulted in a % closure of ~55 ± 7%. MSCs incubated in serum free medium or any of the tumor conditioned mediums did not migrate into the circular gap, and therefore, did not exhibit a chemokinetic response as shown in b). The scale bars shown are 200 μm.

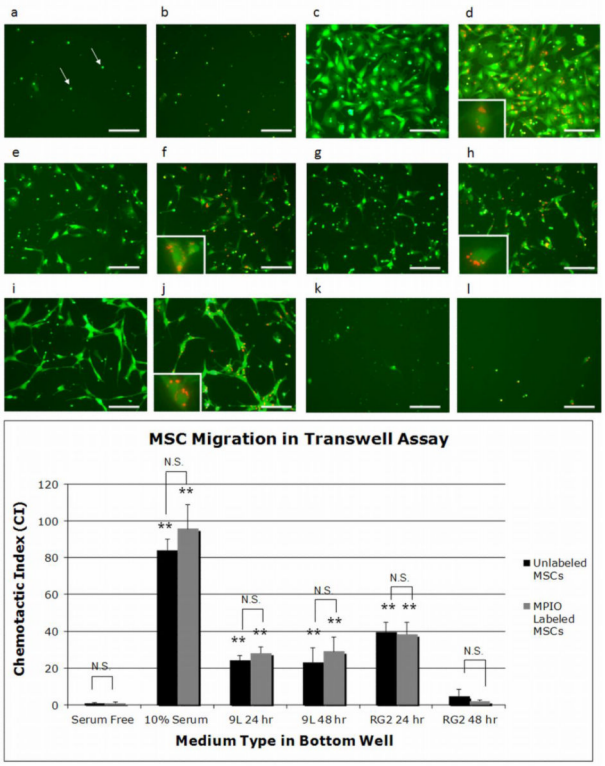

Figure 6.

Fluorescence photomicrographs of chemotactic migration of unlabeled and MPIO labeled MSCs after 17 hours towards a,b) serum free medium c,d) 10% serum containing medium e,f) 9L 24 hour conditioned medium g,h) 9L 48 hour conditioned medium i,j) RG2 24 hour conditioned medium and k,l) RG2 48 hour conditioned medium. Cells are shown in green and MPIOs in red. Each image displays a representative subsection of migrated MSCs on the bottom side of the FluoroBlok membranes. Insets are magnified images of single or small groups of migrated cells containing internalized MPIOs. Pores are marked by white arrows in a). The scale bars shown are 100 μm. The bar graph shows the chemotactic index (CI) for unlabeled and MPIO labeled MSCs in this transwell assay. **$p<0.01$ indicates a highly significant CI compared to serum free medium and N.S. indicates CI pairs that are not significantly different.